THE JOURNAL OF BIOLOGICAL CHEMISTRY VOL. 285, NO. 41, pp. 31704–31712, October 8, 2010

Apical Scaffolding Protein NHERF2 Modulates the Localization of Alternatively Spliced Plasma Membrane Ca^{2+} Pump 2B Variants in Polarized Epithelial Cells*

Received for publication, July 13, 2010 Published, JBC Papers in Press, July 27, 2010, DOI 10.1074/jbc.M110.164137

Rita Padányi[‡], Yuning Xiong[§], Géza Antalffy[‡], Krisztina Lór[‡], Katalin Pászty[¶], Emanuel E. Strehler[§1], and Ágnes Enyedi[‡2]

From the [‡]Department of Molecular Cell Biology, National Blood Center, H-1113 Budapest, Hungary, the [§]Department of Biochemistry and Molecular Biology, Mayo Clinic College of Medicine, Rochester, Minnesota 55905, and the [¶]Membrane Research Group, Semmelweis University, Hungarian Academy of Sciences, H-1067 Budapest, Hungary

The membrane localization of the plasma membrane Ca^{2+}-ATPase isoform 2 (PMCA2) in polarized cells is determined by alternative splicing; the PMCA2w/b splice variant shows apical localization, whereas the PMCA2z/b and PMCA2x/b variants are mostly basolateral. We previously reported that PMCA2b interacts with the PDZ protein Na^+/H^+ exchanger regulatory factor 2 (NHERF2), but the role of this interaction for the specific membrane localization of PMCA2 is not known. Here we show that co-expression of NHERF2 greatly enhanced the apical localization of GFP-tagged PMCA2w/b in polarized Madin-Darby canine kidney cells. GFP-PMCA2z/b was also redirected to the apical membrane by NHERF2, whereas GFP-PMCA2x/b remained exclusively basolateral. In the presence of NHERF2, GFP-PMCA2w/b co-localized with the actin-binding protein ezrin even after disruption of the actin cytoskeleton by cytochalasin D or latrunculin B. Surface biotinylation and fluorescence recovery after photobleaching experiments demonstrated that NHERF2-mediated anchorage to the actin cytoskeleton reduced internalization and lateral mobility of the pump. Our results show that the specific interaction with NHERF2 enhances the apical concentration of PMCA2w/b by anchoring the pump to the apical membrane cytoskeleton. The data also suggest that the x/b splice form of PMCA2 contains a dominant lateral targeting signal, whereas the targeting and localization of the z/b form are more flexible and not fully determined by intrinsic sequence features.

Plasma membrane Ca^{2+}-ATPases (PMCAs)[3] are responsible for maintaining cellular Ca^{2+} homeostasis by removing excess Ca^{2+} from the cytosol. In addition to their housekeeping role, PMCAs also have more specialized tasks in controlling local Ca^{2+}-mediated events. The need for specific Ca^{2+} handling is reflected by the existence of over 20 different PMCA variants in mammals as follows: four separate genes code for PMCA isoforms 1–4, and alternative splicing of the primary transcripts further increases the number of PMCA variants (1).

Earlier work demonstrated that targeting of PMCAs to specific membrane compartments is affected by alternative splicing. Splicing at site A occurs in the region encoding the first intracellular loop where a single exon coding for 12–14 amino acids is either included or excluded in the mature transcripts, producing the "x" and "z" splice variants, respectively. In mammalian PMCA2, two additional exons can be inserted at this site, producing splice variants "w" and "y". The "w" form has the longest insert (45 amino acid residues) in the first intracellular loop, and this appears to target PMCA2 to the apical membrane of polarized cells (2, 3). The shorter forms (x and z) of the pump are localized mostly laterally.

The alternative splice at site C affects the cytosolic C-terminal tail of the PMCA and produces two main splice variants, "a" and "b" (1). All b splice variants contain a PDZ-binding motif (…ETSL or …ETSV) at the C terminus that connects PMCAs to specific scaffolding and signaling proteins such as members of the membrane-associated guanylate kinase family (4, 5) or the Na^+/H^+ exchanger regulatory factor 2 (NHERF2) (6).

PMCA2 is a prominent plasma membrane Ca^{2+} pump of the inner ear (7), specific regions of the brain (8), and lactating mammary gland (9). In some of these places, such as the apical membrane of lactating mammary epithelia, PMCA2w/b is expressed in exceptionally large amounts. A major role of PMCA2w/b in the mammary gland is to provide milk calcium as demonstrated in PMCA2 "knock-out" mice (10). However, it is not yet known how PMCA2w/b is recruited to and concentrated at the apical membrane of these epithelial cells. An earlier study showed that the C-terminal sequence (ETSL) of PMCA2b interacts with the scaffolding protein NHERF2 (6). NHERF proteins are expressed in polarized epithelial cells where they target membrane proteins to the apical cytoskeleton via their ezrin, radixin, moesin (ERM) binding domain (11, 12). NHERF2 has been assigned to play an essential role in establishing the polarity of MDCK epithelial cells (13). Furthermore, NHERF2 interacts with P2Y(1) purinergic receptors (14) as well

* This work was supported, in whole or in part, by National Institutes of Health Grant NS51769 (to E. E. S.). This work was also supported in part by Hungarian Academy of Sciences Grants OTKA K49476, CK 80283, and ETT 215/2009 (to A. E.) and by OTKA Postdoctoral Fellowship D48496 (to R. P.).

[1] Co-senior author. To whom correspondence may be addressed: Mayo Clinic College of Medicine, 200 First St. S.W., Rochester, MN 55905. Tel.: 507-284-9372; Fax: 507-284-2384; E-mail: strehler.emanuel@mayo.edu.

[2] Co-senior author. To whom correspondence may be addressed: National Blood Center, Dept. of Molecular Cell Biology, Diószegi u. 64, H-1113 Budapest, Hungary. Tel./Fax: 36-1-372-4353; E-mail: enyedi@kkk.org.hu.

[3] The abbreviations used are: PMCA, plasma membrane Ca^{2+} pump; ERM, ezrin, radixin, moesin; FRAP, fluorescence recovery after photobleaching; MDCK, Madin-Darby canine kidney; NHERF, Na^+/H^+ exchanger regulatory factor; DPBS, Dulbecco's modified PBS; TRITC, tetramethylrhodamine isothiocyanate.

as mGluR5 (15) in the brain; and this interaction was found to prolong receptor-mediated calcium mobilization.

To determine whether interaction with NHERF2 affects the targeting of the splice site A variants of PMCA2b in polarized cells, we used the MDCK model system and found that NHERF2 greatly enhanced the concentration of PMCA2w/b at the apical membrane by anchoring it to the apical cytoskeleton. Fluorescence recovery after photobleaching (FRAP) studies suggest that the NHERF2-mediated anchorage to the cytoskeleton immobilizes and thereby stabilizes the pump in the apical membrane. We further demonstrate that NHERF2 can redirect PMCA2z/b from the lateral to the apical plasma membrane in MDCK cells, suggesting that this splice variant lacks a firm membrane localization signal. In contrast, PMCA2x/b localizes exclusively to the lateral membrane regardless of the presence of NHERF2, suggesting that the x-splice insert contributes a strong lateral localization signal. Together, our data provide insights into the mechanism of PMCA2w/b clustering that may occur at specific membrane compartments such as the apical epithelial membrane of the lactating mammary gland.

EXPERIMENTAL PROCEDURES

Reagents and Antibodies—FuGENE 6 transfection reagent was obtained from Roche Applied Science, and Lipofectamine™ was from Invitrogen. DMEM and Opti-MEM were obtained from Invitrogen. Polyclonal anti-PMCA2 antibody NR2 (16) was used at a dilution of 1:100 for indirect immunofluorescence staining and 1:600 for immunoblotting. Affinity-purified polyclonal anti-NHERF2 antibody Ab720 (6) was used at a concentration of 0.5 μg/ml. Monoclonal anti-ezrin antibody was from BD Biosciences and used at a dilution of 1:100. Chicken polyclonal anti-Na^+/K^+-ATPase antibody was from Chemicon International (Temecula, CA) and used at a dilution of 1:250. TRITC-phalloidin (used at 0.1 μg/ml) was obtained from Sigma. Alexa Fluor 488-, 594-, and 633-conjugated goat anti-mouse and anti-rabbit IgGs and Alexa Fluor 594-conjugated goat anti-chicken IgG were obtained from Invitrogen. All other chemicals used were of reagent grade.

Plasmid Constructs—Plasmids GFP-PMCA2w/b, GFP-PMCA2w/bΔ6, GFP-PMCA2x/b, and GFP-PMCA2z/b for expression of human GFP-tagged PMCA2b splice forms in mammalian cells have been described (2). The mammalian expression construct for NHERF2 was a kind gift from Dr. Randy Hall (Emory University, Atlanta) and has been described previously (17, 18).

Cell Culture and Transfection—MDCKII and HeLa epithelial cells were grown in Dulbecco's modified Eagle's medium (DMEM) supplemented with 10% (v/v) fetal bovine serum, 100 units/ml penicillin, 100 μg/ml streptomycin, and 2 mM L-glutamine. Cells were kept at 37 °C and 5% CO_2 in a humidified atmosphere. For transient transfection, cells were cultured to reach 80–90% confluency and transfected with plasmid DNA using FuGENE 6 transfection reagent according to the manufacturer's protocol.

Indirect Immunofluorescence Staining—For confocal imaging, MDCK cells were grown on 8-well Nunc Lab-Tek Chambered Coverglass (Nalge Nunc International, Rochester, NY) or on glass coverslips in DMEM containing 10% fetal bovine serum. 48 h after transfection, cells were rinsed with Dulbecco's modified PBS (DPBS), fixed for 10 min at 37 °C in 4% paraformaldehyde, and permeabilized for 2 min in 0.2% Triton X-100/DPBS. After three washes with DPBS, cells were blocked for 1 h at room temperature in blocking buffer (DPBS containing 2 mg/ml bovine serum albumin, 1% fish gelatin, 0.1% Triton X-100, and 5% goat serum). Samples were then incubated for 1 h at room temperature with primary antibodies (affinity-purified rabbit polyclonal anti-PMCA2 antibody, rabbit polyclonal anti-NHERF2 antibody, chicken polyclonal anti-Na^+/K^+-ATPase antibody, and/or monoclonal anti-ezrin antibody). After three washes in DPBS, cells were incubated for 1 h at room temperature with Alexa Fluor 488-, Alexa Fluor 594-, or Alexa Fluor 633-conjugated goat anti-mouse and anti-rabbit or Alexa Fluor 594-conjugated goat anti-chicken secondary antibodies at a dilution of 1:250. In some cases, TRITC/phalloidin (0.1 μg/ml in DPBS) was added after incubation with secondary antibody. After final washing, glass coverslips were mounted in Prolong mounting media (Molecular Probes).

Image Acquisition—Samples were observed with an Olympus IX-81 laser scanning confocal microscope and Fluoview FV500 (version 4.1) software using an Olympus PLAPO ×60 (1.4) oil immersion objective (Olympus Europe GmbH, Hamburg, Germany) or with a Zeiss LSM510 microscope using an Apochromat ×63 oil immersion objective and using LSM510 software version 2.8 (Zeiss). For multichannel imaging, fluorescent dyes were imaged sequentially, and the wavelength of light was collected. Each detection channel was set such that no detectable bleed through occurred between the different channels. Images were imported and edited using Adobe Photoshop 5.0 and Gimp 2.6.2.

Image Processing and Quantification—Quantification of apical membrane localization was done as described previously (2). Images of the apical and middle sections of 15–20 representative cells from each transfection were collected, applying the same detector gain, zoom, amplitude offset and gain, transmission percent, pinhole size, and scan speed for each image. The ratio of mean PMCA fluorescence intensities of equal regions of interest in apical *versus* middle sections of cells was determined. These numbers were displayed in a bar graph showing the averages of the mean fluorescence intensities for each of the PMCA2 transfections.

Pearson's correlation coefficients (r) were used to quantify the extent of co-localization between two labelings and were calculated with ImageJ 1.36b using the plug-in module Co-localization Finder (C. Laummoneire and J. Mutterer, Strasbourg, France). The minimum ratio for pixel intensity between the two channels was set to 0.4. Pearson's correlation values represent the means ± S.D. of calculations from 15 to 20 cells of three independent experiments. Means ± S.D. were calculated using Microsoft Excel software (Microsoft, Seattle).

Live Cell Confocal Imaging and FRAP Studies—MDCK cells were cultured in DMEM on 8-well Nunc Lab-Tek Chambered Coverglass for 48 h and transfected with DNA constructs (GFP-PMCA2w/b or GFP-PMCA2w/bΔ6 together or without NHERF2). Time-lapse sequences were recorded with Fluoview Tiempo (version 4.3) time course software at room temperature using an Olympus IX-81 laser scanning confocal micro-

scope. FRAP experiments were performed 48 h after transfection using the 488 nm line of an argon laser with a 60 × 1.4 NA oil immersion objective. A defined segment of the apical surface of the cell (circular spot with a diameter of about 2 μm) was photobleached by three iterations at full laser power (100% power) at ×10 magnification. Pre- and post-bleach images were acquired every 3 s over a 5-min time period at low laser intensity (3% power). Mean fluorescence intensity data from regions of interest and nonbleached regions were collected using Fluoview FV500 (version 4.1) imaging software. Data were imported into Microsoft Excel software, normalized to the pre-bleach intensities and corrected for acquisition bleaching caused by the fluorescence recording process using double normalization methods (19). The kinetics of recovery were determined by exponential fitting of the average data using the nonlinear regression algorithm of PRISM software version 3.0 (GraphPad Software Inc., San Diego) as described previously (20).

Cell-surface Biotinylation Assay for Endocytosis and Recycling—This assay was performed following the procedure of the cell-surface protein biotinylation kit (catalog no. 89881, Pierce) with minor modifications. Transfected HeLa cells were washed two times with ice-cold BupH™ PBS (pH 7.2, Pierce). Cell-surface proteins were labeled by incubation on a rocking platform with 0.25 mg/ml membrane-impermeable sulfosuccinimidyl-2-(biotinamido)ethyl-1,3-dithiopropionate (sulfo-NHS-SS-biotin) in PBS for 30 min on ice. Biotinylation was stopped by adding Quenching Solution (Pierce) to each flask. The cells were then washed and lysed, and the biotinylated proteins were collected as described below (input) or were incubated at 37 °C for the indicated periods of time to allow recycling of cell surface proteins. To measure recycling of endocytosed proteins, biotin was removed from the cell surface by incubation with 50 mM L-glutathione (Sigma) for 30 min on ice. Glutathione was quenched by 5.5 mM iodoacetamide (Sigma) followed by one further wash in PBS. After glutathione stripping, cells were scraped in PBS containing protease inhibitors (0.1 mM Pefabloc™, 10 μg/ml leupeptin, 20 μg/ml aprotinin), sedimented by centrifugation (4000 × *g*, 4 °C for 3 min), and washed again with BupH™ TBS. After centrifugation, cells were lysed by Lysis Buffer containing 0.1 mM Pefabloc™, 10 μg/ml leupeptin, 20 μg/ml aprotinin on ice. The cell extract was centrifuged at 10,000 × *g* for 5 min, and the supernatant was incubated with immobilized NeutrAvidin™ gel beads (Pierce) for 60 min at room temperature with end-over-end mixing to precipitate the biotinylated proteins. Subsequently, the beads were washed five times with Wash Buffer (Pierce), and proteins were eluted from the beads with SDS sample buffer containing 50 mM fresh dithiothreitol. The precipitates were resolved by SDS-PAGE and transferred onto nitrocellulose, followed by Western blotting.

RESULTS

NHERF2 Enhances Apical Localization of PMCA2w/b—To test if interaction with NHERF2 affected the apical/lateral localization of PMCA2w/b, we transiently expressed GFP-tagged PMCA2w/b with or without NHERF2 in MDCK cells and studied its localization with laser scanning confocal microscopy. We used GFP-tagged PMCA2 constructs throughout this study because previous work had shown that the localization of N-terminally GFP-tagged PMCAs faithfully reflects the localization of the corresponding untagged pumps in polarized MDCK cells (2). The typical apical plus basolateral distribution of GFP-PMCA2w/b (Fig. 1*A*) changed remarkably when NHERF2 was co-expressed, and it now showed a more pronounced apical localization of the pump (Fig. 1*B*). The *upper panels* of Fig. 1*B* show a perfect match of the NHERF2 and GFP (PMCA2w/b) signals, and the *lower panels* show that the GFP (PMCA2w/b) signal is clearly separated from the signal of the basal/lateral Na^+/K^+-ATPase marker. Quantitative analysis revealed that the ratio of apical to lateral fluorescence intensity of the GFP signal increased 2-fold when NHERF2 was co-expressed with GFP-PMCA2w/b (Fig. 1*C*). In contrast, a truncated mutant (GFP-PMCA2w/bΔ6) lacking the PDZ-binding C-terminal tail showed no change in the ratio of apical to lateral localization when co-expressed with NHERF2 (Fig. 1*C*). This demonstrates that the NHERF2-induced increase in the apical localization of PMCA2w/b is strictly dependent on the PDZ-binding motif in the C-terminal tail of the PMCA. These data suggest that PDZ domain-mediated interactions with NHERF2 enhance the stability of PMCA2w/b at the apical plasma membrane. We next tested if this stabilization occurs by tethering the pump to the actin cytoskeleton via the scaffolding protein NHERF2.

NHERF2 Links PMCA2w/b to the Actin Cytoskeleton through Ezrin—NHERF proteins are thought to connect apical membrane proteins to the actin cytoskeleton by binding to ERM proteins via their ERM binding C-terminal domain (21–23). To test if NHERF2 connects PMCA2w/b to the actin cytoskeleton, we co-expressed GFP-PMCA2w/b with NHERF2 in MDCK cells and labeled the actin filaments with TRITC/phalloidin. Phalloidin detected actin-containing apical patches in polarized MDCK cells and showed strong co-localization with GFP-PMCA2w/b in the presence of NHERF2 (Fig. 2, *panels A1–A4*). In fact, the pattern of the apical actin patches (Fig. 2, *panel A3*) was strikingly similar to that of the GFP-PMCA2w/b (Fig. 2, *panel A1*) and NHERF2 (Fig. 2, *panel A2*) signals. The calculated Pearson's co-localization coefficient for actin and GFP-PMCA2w/b was nearly as high as for GFP-PMCA2w/b and NHERF2 (Fig. 2*C*) and indicated co-localization of these proteins. In contrast, the degree of co-localization between GFP-PMCA2w/b and the apical actin cytoskeleton was low when the pump was expressed without NHERF2 (Fig. 2*C*), most probably because of the relatively low endogenous NHERF2 expression level of the MDCK cells.

Because NHERF proteins interact with the actin cytoskeleton through ERM proteins, we further tested if the PMCA and NHERF2 co-localized with the endogenous actin-binding protein ezrin (Fig. 2, *panels B1–B4*). Both the similar staining pattern and the calculated Pearson's correlation coefficients (Fig. 2*C*) indicated an interaction between the three proteins, PMCA2w/b, NHERF2, and ezrin, at the apical membrane. Again, very little if any co-localization with ezrin was detected when the pump was expressed alone, demonstrating that NHERF2 was essential to connect PMCA2w/b to ezrin (Fig. 2*C*).

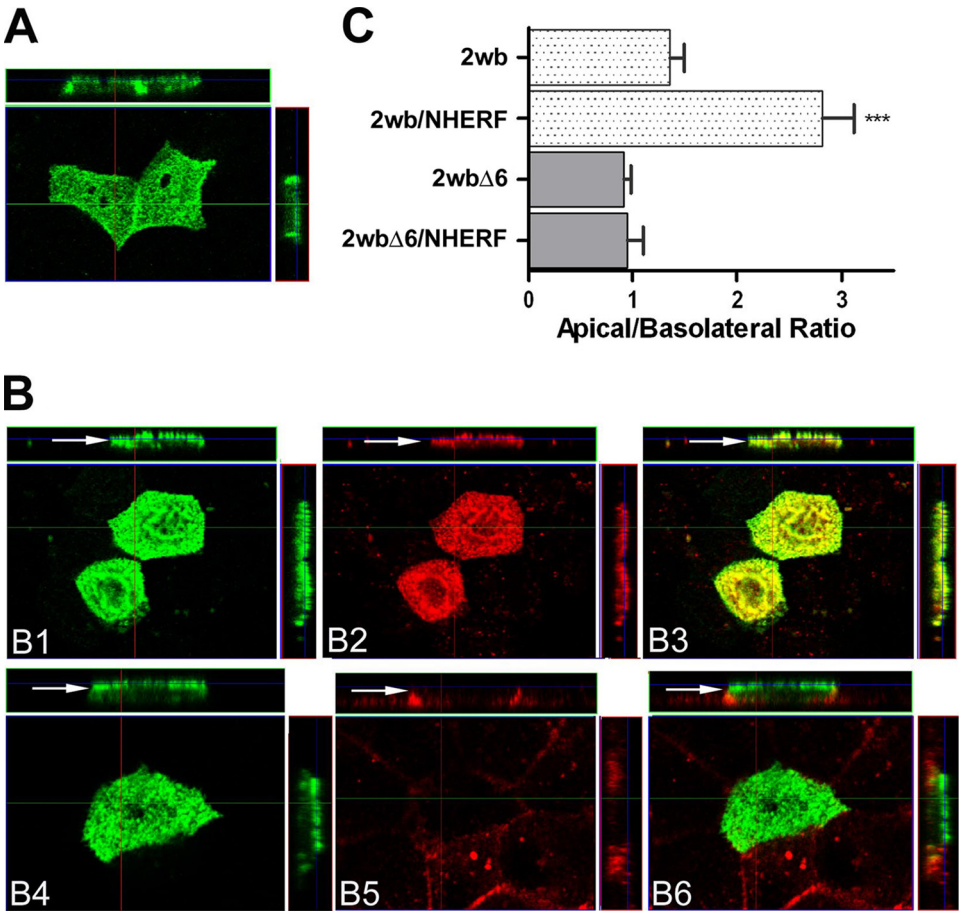

FIGURE 1. **NHERF2 enhances apical localization of PMCA2w/b.** GFP-PMCA2w/b was transiently expressed in MDCK cells without (*A*) or with (*B*) NHERF2. PMCA localization was detected by confocal microscopy. Cells were stained with anti-NHERF2 antibody (*panel B2*) or basolateral Na^+/K^+-ATPase α-subunit antibody (*panel B5*). *Panels B1* and *B4* show the distribution of the GFP signal; *panels B3* and *B6* are merged images of *panels B1* and *B2* and *panels B4* and *B5*, respectively. Note co-localization of the GFP-PMCA2w/b and NHERF2 signals in the apical membrane in the merged image *panel B3*, and the separation of *green* (GFP-PMCA2w/b, apical) and *red* (Na^+/K^+-ATPase, basolateral) fluorescence in the merged image *panel B6*. *Arrows* in xz sections on the *top* of each panel indicate the apical location where the xy sections were taken. The *bar graph* in *C* shows the ratio of mean PMCA fluorescence intensities of equal regions of interest in apical *versus* middle sections of cells expressing GFP-PMCA2w/b (2wb), C-terminally truncated GFP-PMCA2w/bΔ6 (2wbΔ6), or either of these pumps together with NHERF2 (2wb/NHERF and 2wbΔ6/NHERF). Fluorescence quantification was performed as described under "Experimental Procedures." Removing the C-terminal residues from PMCA2w/b suppresses the effect of NHERF2 on the redistribution of the pump toward the apical region (compare the *last two bars* in *C*). Values represent the mean ± S.D. of calculations from 15 to 20 cells of three independent experiments. ***, $p < 0.05$ *versus* 2wb.

To further analyze the interactions mediated by NHERF2 to anchor PMCA2w/b to the apical membrane skeleton, we treated cells before fixing with cytochalasin D, a fungal toxin that depolymerizes actin microfilaments. Fig. 2, *panels A5–A8,* shows that cytochalasin D treatment induced aggregation of actin, accompanied by a marked loss of the co-localization of actin with PMCA2w/b and NHERF2. Remarkably, however, the NHERF2-mediated PMCA2w/b-ezrin complex was not disrupted by the cytochalasin D treatment; the three proteins showed strong co-localization in distinct large patches at or near the apical plasma membrane after treatment (Fig. 2, *panels B5–B8,* and *C*). We observed an essentially identical effect on the distribution of actin filaments, PMCA2w/b, and ezrin when cells were treated with 1 μM latrunculin B for 30 min (Fig. 2, *panels A9–A12* and *B9–B12*). Our results support a tight interaction between these proteins (PMCA2w/b-NHERF2-ezrin) that persists even when the actin cytoskeleton is disrupted. These data indicate that NHERF2 anchors PMCA2w/b to the actin cytoskeleton through ezrin (Fig. 2*D*) and suggest that NHERF2 can redistribute PMCA2w/b to the apical membrane by increasing its stability in that compartment.

PMCA2w/b Anchored by NHERF2 Has Limited Mobility in the Plasma Membrane—To test if anchorage to the apical cytoskeleton affects the lateral mobility of PMCA2w/b, we expressed GFP-PMCA2w/b in MDCK cells with or without NHERF2 and monitored the mobility of the pump by FRAP (Fig. 3*A*). Recovery within the bleached region was normalized to the prebleach values using the double normalization method (19) to correct for the acquisition bleaching. The recovery kinetic parameters were determined by exponential fitting of the average data as described earlier (20). Fig. 3 shows that recovery of the GFP-PMCA2w/b-associated fluorescence after photobleaching was not complete when the protein was co-expressed with NHERF2; only an average of 44 ± 9% of the fluorescence reappeared after a 300-s time period. These findings suggest that a major fraction of the apical PMCA2w/b (over 50%) was virtually immobile. In contrast, the relative fluorescence recovery of the GFP signal was 87 ± 24% when GFP-PMCA2w/b was expressed alone, indicating a much higher mobility of the pump in the absence of NHERF2. The truncated mutant (GFP-PMCA2w/bΔ6) lacking the PDZ-binding C-terminal residues also showed nearly complete fluorescence recovery with or without NHERF2 (Fig. 3*A* and Table 1), indicating that PDZ domain-dependent interaction with NHERF2 is essential for reducing the mobility of the pump.

The confocal images in Fig. 2 suggested that actin cytoskeleton disruption with cytochalasin D or latrunculin B rendered PMCA2w/b, NHERF2, and ezrin into large patches, although this multiprotein complex seemed to be separated from the disorganized actin filaments. Therefore, we tested how disruption of the actin cytoskeleton by latrunculin B treatment affects membrane mobility of GFP-PMCA2w/b. GFP-PMCA2w/b was expressed with or without NHERF2 in MDCK cells and treated for 30 min with 1 μM latrunculin B before FRAP mobility measurements. Fig. 3*B* shows that latrunculin treatment did not substantially change the recovery curves. Fitting the recovery curves with double exponential equations yielded only slightly

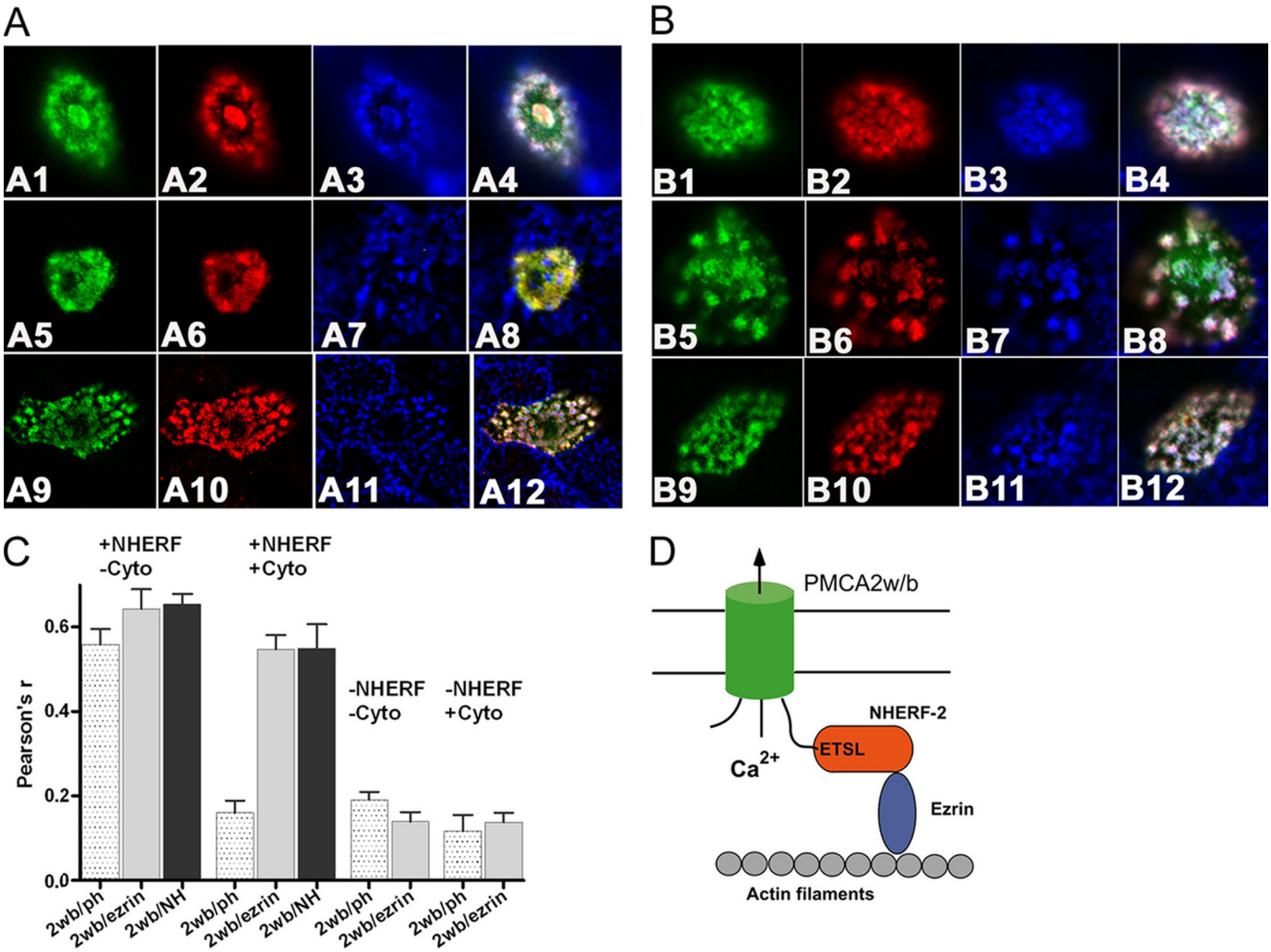

FIGURE 2. **NHERF2 anchors PMCA2w/b to the actin cytoskeleton beneath the apical membrane of polarized MDCK cells.** *A* and *B*, MDCK cells co-expressing GFP-PMCA2w/b (*green*) and NHERF2 were formaldehyde- fixed, permeabilized with Triton X-100, and stained with anti-NHERF2 antibody (*red*) and either TRITC-labeled phalloidin (*blue* in *A panels*) or anti-ezrin antibody (*blue* in *B panels*). In *panels A5–A8* and *B5–B8*, cells were treated with 2.5 μM cytochalasin D for 10 min and in *panels A9–A12* and *B9–B12* with 1 μM latrunculin B for 30 min before the addition of formaldehyde. The apical sections of typical cells expressing the appropriate constructs are shown. *Panels A4, A8, A12, B4, B8,* and *B12* show merged images, where *white* indicates overlap of the *green, red,* and *blue* staining. *C*, Pearson's co-localization coefficients of the GFP-PMCA2w/b (*2wb*), NHERF2 (*NH*), ezrin, and phalloidin (*ph*) signals in MDCK cells without (−*Cyto*) or with (+*Cyto*) cytochalasin D treatment were determined as described under "Experimental Procedures." Values represent the mean ± S.D. of calculations from 15 to 20 cells of three independent experiments. *D*, schematic showing anchorage of PMCA2w/b to the apical actin cytoskeleton by NHERF2 via ezrin. PMCA2w/b binds via its C-terminal ETSL sequence to the PDZ protein NHERF2, which interacts through its ERM domain with ezrin.

different time constants, and there were no significant differences between the mobile fractions of GFP-PMCA2w/b in cells treated or not with latrunculin B (Fig. 3*B* and Table 1). This experiment demonstrates that disruption of the actin cytoskeleton does not induce release of PMCA molecules from the complex, and thus the GFP-PMCA2w/b-NHERF2 patches remained immobile.

NHERF2 Increases Membrane Residence Time of PMCA2w/b—To determine whether the reduced lateral mobility correlates with an increased membrane residence time of PMCA2w/b, we performed a surface biotinylation assay to determine plasma membrane levels of PMCA2w/b in the absence and presence of NHERF2. Because MDCK cells transfect with low efficiency, HeLa cells were transiently transfected with full-length GFP-PMCA2w/b with or without NHERF2 or with GFP-PMCA2w/bΔ6 lacking the six C-terminal amino acids. Two days after transfection, cells were labeled with sulfo-NHS-SS-biotin on ice, and total biotinylated plasma membrane PMCA levels were determined (Fig. 4, *input lanes*). Then cells were warmed to 37 °C and treated after various times with reduced glutathione to remove the surface-exposed biotin. The amount of internalized, biotinylated PMCA protein was determined by Western blotting at the times indicated. Fig. 4 shows that a much larger fraction of the pump remained biotinylated when the PDZ-binding C-terminal residues were removed, indicating that the truncated pump internalized more rapidly than the full-length PMCA2w/b. Co-expression of full-length PMCA2w/b with NHERF2, on the other hand, substantially reduced PMCA internalization as glutathione treatment removed nearly all (only about 10% retained) biotin from the PMCA even after 20 min of incubation at 37 °C. In summary, the FRAP and biotinylation assays together suggest that NHERF2 immobilizes

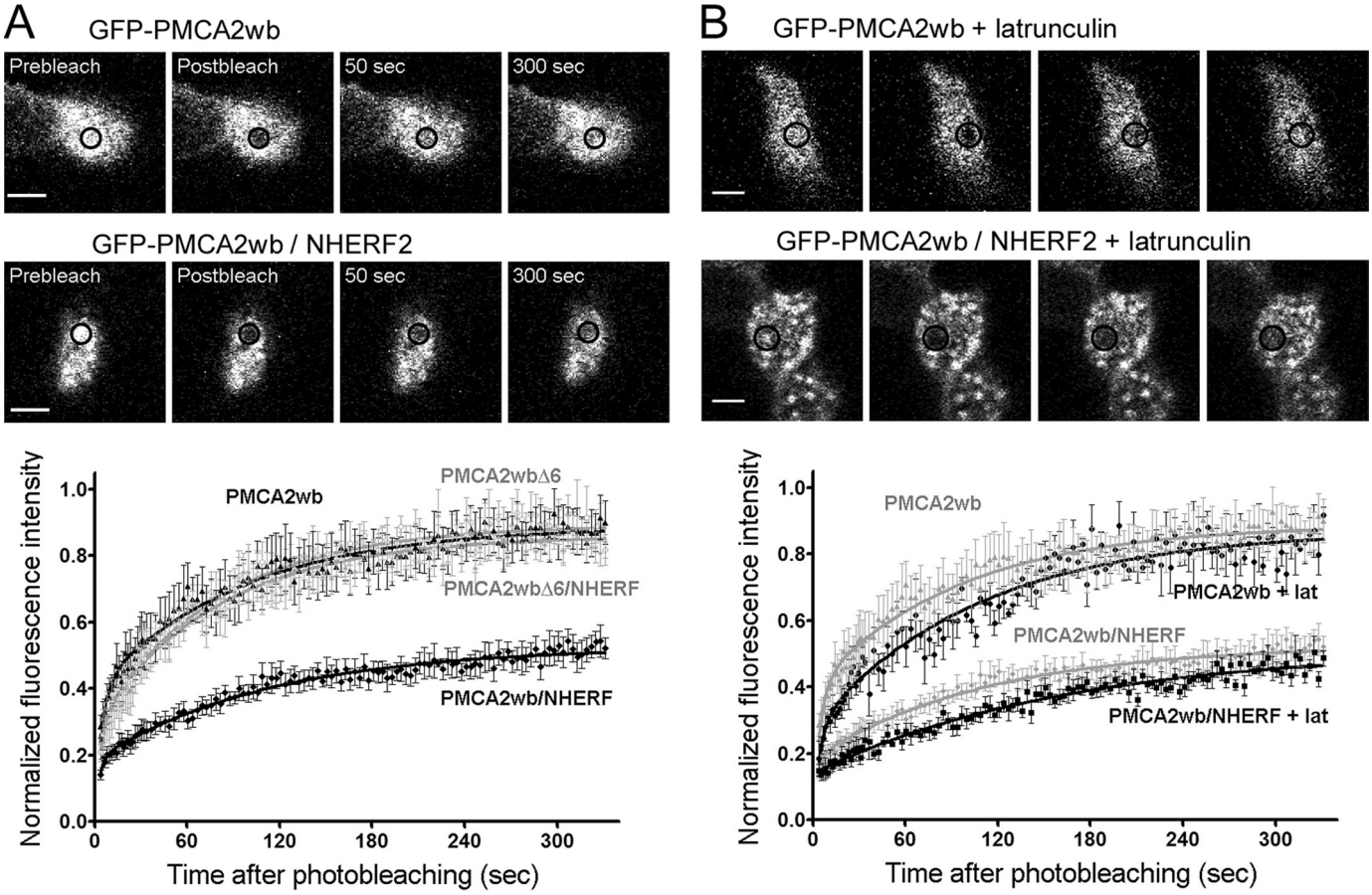

FIGURE 3. **NHERF2 greatly reduces the lateral mobility of GFP-PMCA2w/b in MDCK cells.** Confocal images of GFP fluorescence at the apical surface of live MDCK cells expressing GFP-PMCA2w/b alone or together with NHERF2 are as indicated. The *circled* region of interest with a diameter of 2.6 μm was bleached by a high intensity argon laser beam at 488 nm. The fluorescence recovery within the region of interest was followed by scanning every 3 s for 5 min. The fluorescence at each time point after bleaching was normalized to the pre-bleach intensity and corrected for acquisition bleaching. *A*, *black lines* indicate the recovery curves of GFP-PMCA2w/b in the absence (*triangles*) and presence (*diamonds*) of NHERF2. *Gray lines* indicate the recovery curves of the C-terminally truncated GFP-PMCA2w/bΔ6 mutant in the absence (*open circles*) and presence (*asterisks*) of NHERF2. *B* shows confocal images of FRAP experiments performed on MDCK cells after 1 μM latrunculin B treatment for 30 min at 37 °C. In the *graph*, control curves are shown in *gray* (GFP-PMCA2w/b without NHERF2 (*triangles*) and with NHERF2 (*diamonds*)). *Black lines* indicate the recovery curves of GFP-PMCA2w/b in the absence (*circles*) and presence of NHERF2 (*squares*) after latrunculin (*Lat*) treatment. The *solid lines* through the data are exponential fits to the averaged data of five experiments ± S.E. *Scale bars,* 5 μm.

TABLE 1

The mobile fraction of PMCA2w/b is greatly reduced by NHERF2 expression

The mobile fraction of each construct +/− NHERF2 was determined using the data shown in Fig. 3. Data are shown as mean ± S.D. *n*, number of measurements.

	Treatment	Mobile fraction	*n*
		%	
GFP-PMCA2w/b	None	87 ± 24[a]	7
GFP-PMCA2w/b + NHERF2	None	44 ± 10[a,b]	7
GFP-PMCA2w/bΔ6	None	77 ± 12	5
GFP-PMCA2w/bΔ6 + NHERF2	None	78 ± 14[b]	4
GFP-PMCA2w/b	Latrunculin	90 ± 4[c]	3
GFP-PMCA2w/b + NHERF2	Latrunculin	40 ± 8[c]	8

[a] $p < 0.01$.
[b] $p < 0.02$ for Student's *t* test of two-tailed hypothesis, relative to the group identified by the same symbol.
[c] $p < 0.01$.

PMCA2w/b in the apical membrane, resulting in slower endocytic trafficking and an increased membrane residence time of the pump.

NHERF2 Recruits PMCA2z/b but Not PMCA2x/b to the Apical Membrane—Our previous study (2) showed that the A-site splice forms of PMCA2 are differently located in polarized MDCK cells; although PMCA2w/b showed prominent apical localization in addition to basal/lateral location, PMCA2z/b and -2x/b were found in the basal/lateral membrane. Because the NHERF2-binding C-terminal sequence is equally present in all A-site splice variants of PMCA2b, we tested whether co-expression of NHERF2 affected targeting of the x and z splice variants of PMCA2b. As shown in Fig. 5, NHERF2 induced a substantial redistribution of GFP-PMCA2z/b to the apical membrane (Fig. 5*A*), but it was unable to recruit GFP-PMCA2x/b from the lateral to the apical membrane (Fig. 5*B*). For PMCA2z/b, co-localization was detected with NHERF2 at the apical membrane (Fig. 5, *A1–A3*) and with the endogenous Na^+/K^+-ATPase at the lateral membrane (Fig. 5, *A4–A6*). In contrast, GFP-tagged PMCA2x/b retained its basolateral position; the GFP signal was clearly separated from the NHERF2 signal at the apical membrane (Fig. 5, *B1–B3*), but it correlated well with the signal of the Na^+/K^+-ATPase at the lateral membrane (Fig. 5, *B4–B6*). Quantitative analysis revealed that the ratio of apical to lateral fluorescence intensity of the GFP-PMCA2z/b signal increased in the presence of NHERF2 to about 1:1, although the apical concentration of GFP-PMCA2w/b was still much higher in the presence of NHERF2

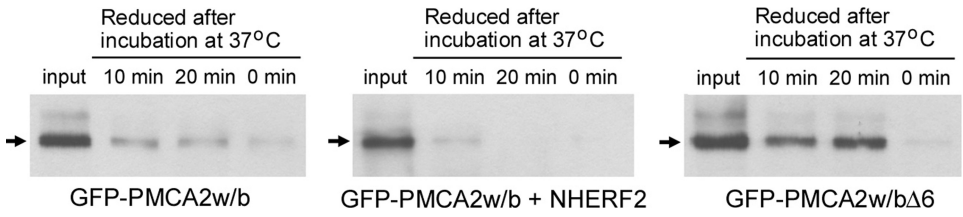

FIGURE 4. **NHERF-2 reduces the recycling of PMCA2w/b.** Cells transfected with the proteins indicated on *top* of each panel were surface-biotinylated on ice and then washed and collected (*input*) or incubated at 37 °C for the indicated times to allow endocytosis of PMCA. After glutathione stripping, cells were lysed, and biotinylated proteins were recovered on streptavidin beads. Wild type PMCA2w/b (*left panel*), NHERF2-associated PMCA2w/b (*middle panel*), and the truncated PMCA2w/bΔ6 (*right panel*) were resolved and visualized by Western blotting (*arrows*), using anti-PMCA antibody 5F10. Glutathione stripping immediately after biotinylation efficiently removed all surface-biotinylated proteins (*lanes* labeled *0 min*). Incubation of cells at 37 °C for 10 or 20 min allowed the recycling of PMCA. Endocytosis of the truncated PMCA2w/bΔ6 was more pronounced (65 ± 6% of input proteins were recovered after 20 min) than that of the wild type PMCA2w/b (26 ± 9% recovery after 20 min) or the NHERF2-associated PMCA2w/b (10 ± 1% recovery after 20 min). Quantified data represent the average of three independent experiments.

(Fig. 5*C*). NHERF2 did not affect localization of PMCA2x/b, which retained its lateral position. These data show that NHERF2 can modify the membrane distribution of both the w and z splice variants but is unable to overcome the strong basolateral targeting/retention signal in PMCA2x/b.

DISCUSSION

Alternative splicing and interactions with specific scaffolding proteins underlie the flexibility of PMCA2 variants to localize in different membrane domains, allowing them to perform specific cellular functions in handling local Ca^{2+} loads. Indeed, PMCA2 is found in highly specialized plasma membrane compartments; the w splice insert at site A, unique to PMCA2, has been shown to direct this pump to the apical stereocilia of cochlear and vestibular hair cells (3, 24) or to the apical membrane of breast epithelial cells in the lactating mammary gland (9). The b splice at site C, on the other hand, provides the PMCA2 with a C-tail ending with the PDZ domain-binding sequence …LETSL that allows the pump to interact with scaffolding proteins such as members of the membrane-associated guanylate kinase family or NHERF2.

Previous studies using GFP-tagged constructs showed that the z and x forms of PMCA2 localized to the basal and lateral membranes of MDCK cells, whereas the w form displayed prominent apical localization, in addition to some lateral staining (2, 3). Because GFP-tagged and -untagged PMCA2 splice variants are identically localized in transiently transfected MDCK cells and stably transfected cell lines (2, 25), we used GFP-tagged constructs to determine the effect of NHERF2 on the membrane distribution of the PMCA2b splice site A variants.

Our data show that NHERF2 greatly enhanced the apical localization of GFP-PMCA2w/b and recruited a sizable fraction of GFP-PMCA2z/b to the apical membrane. Remarkably, however, NHERF2 could not alter the lateral localization of the x splice form of PMCA2b. The only difference between the x and the z variant is the presence of a short 14-amino acid insert in the first cytosolic loop of the x variant. This insert must therefore contribute significantly to the basolateral localization of the PMCA2x/b, and it seems to protect the pump against the redistributing effect of the apical scaffold protein NHERF2. Interestingly, the x variants of other PMCA isoforms (*e.g.* PMCA4x/b and PMCA1x/b) are also strictly localized to the basolateral membrane in MDCK cells and in rat hair cells (3, 26, 27), although a recent report indicates that PMCA1 (likely PMCA1x/b) is also found in the apical membrane in mouse parotic acinar cells (28). In contrast, the NHERF2-induced partial redistribution of PMCA2z/b from the basal/lateral to the apical membrane indicates that the z forms do not contain a "dominant" basolateral localization signal and instead remain flexible to alter their membrane distribution. How the short x-insert stabilizes the basal/lateral localization of the pump in MDCK cells remains to be determined. The inserted amino acid sequence (GKMQDGNVDASQSK) may provide a new recognition domain for specific protein interactions with a basal/lateral anchoring protein and/or could impose long range structural changes in the cytosolic loop to enable such interactions.

NHERF proteins have previously been shown to promote apical localization, retention, and recycling of several other membrane proteins, including the Na^+/H^+ exchanger NHE3 (23, 29), the cystic fibrosis transmembrane conductance regulator (30–32), the sodium-phosphate co-transporter type IIa (33, 34), and diverse G protein-coupled receptors (17, 35–38). Of interest to this study, NHERF2 and its target, podocalyxin/gp135, are involved in the establishment of epithelial membrane polarity by forming an early apical scaffold during polarization of MDCK cells (13). PMCA2b (as well as PMCA1b) interacts selectively with NHERF2 over NHERF1 (6, 39). The selectivity of NHERFs for different targets might help separate signaling complexes in the plasma membrane and thereby assist cells in organizing different Ca^{2+}-dependent mechanisms into spatially discrete Ca^{2+} signaling domains.

NHERF2 increases the amount of apical PMCA2w/b by recruiting the pump to the apical domain by virtue of its specific PDZ domain interaction, as well as by tethering the pump to the subapical actin cytoskeleton via ezrin. The linkage to the actin cytoskeleton decreased the lateral mobility (as demonstrated by FRAP) and increased membrane retention of the pump by reducing its rate of internalization (as demonstrated by surface biotinylation). Disruption of the actin filament network resulted in decreased co-localization of PMCA2w/b with actin, but the pump still co-localized with NHERF2 and ezrin in large apical patches. The NHERF2-ezrin-actin cytoskeleton interaction might play an essential role in retaining the pump in the apical membrane, whereas the immobility of the large PMCA2w/b-containing patches after latrunculin treatment indicates the relative stability of the multiprotein complex even in the absence of an intact actin filament network. This effect of NHERF2 is reminiscent of the role of NHERF1 in decreasing ligand-induced endocytosis and lateral membrane diffusion of the parathyroid hormone receptor (37, 38) and of NHERF1/2 in

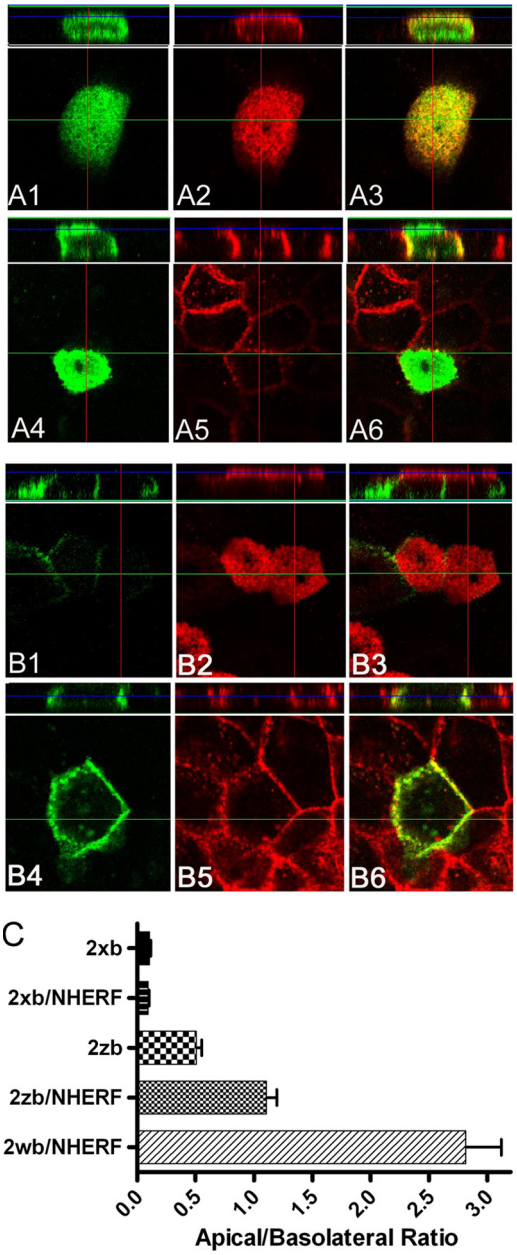

FIGURE 5. **Co-transfection with NHERF2 alters the localization of PMCA2z/b but not PMCA2x/b in polarized MDCK cells.** GFP-PMCA2z/b (*A panels*) or GFP-PMCA2x/b (*B panels*) was co-expressed with NHERF2 in MDCK cells, and the localization of the two proteins was determined by confocal microscopy. NHERF2 was visualized using anti-NHERF antibody (*A2* and *B2*, *red*). Cells were also stained with an antibody against the basolateral Na^+/K^+-ATPase α-subunit (*A5* and *B5*, *red*). Merged images are shown on the *right* (*A3, A6, B3,* and *B6*). Apical xy sections are shown in the *en face* views in *A1–A6* and *B1–B3*, whereas subapical xy sections are shown in *B4–B6*. Corresponding xz sections are shown on *top* of each image. GFP-PMCA2z/b and NHERF2 localization partially overlap at the apical membrane (*A1–A3*), in contrast to the complete separation of GFP-PMCA2x/b and NHERF2 in the lateral and apical domains, respectively (*B1–B3*). Both GFP-PMCA2z/b (xz sections in *A4–A6*) and GFP-PMCA2x/b (*B4–B6*) show substantial co-localization with the basolateral marker Na^+/K^+-ATPase α-subunit. *C,* fluorescence quantification was performed as described under "Experimental Procedures." Values represent the mean ± S.E. of 15–20 cells from three independent experiments.

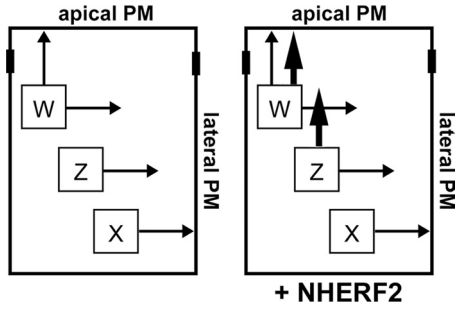

FIGURE 6. **Scheme illustrating the effect of NHERF2 on the cellular distribution of PMCA2b A-splice variants.** *Black arrows* indicate the targeting of PMCA2b variants (W, PMCA2w/b; Z, PMCA2z/b; X, PMCA2x/b) in polarized MDCK cells. Under control conditions (*left panel*), only PMCA2w/b shows prominent targeting to the apical plasma membrane (*apical PM*). Upon NHERF2 expression (*right panel*), apical PMCA2w/b is greatly enhanced, and PMCA2z/b is recruited to the apical membrane (indicated by the *thick arrows*), whereas PMCA2x/b is unaffected and stays in the lateral membrane.

limiting membrane diffusion of NHE3 and cystic fibrosis transmembrane regulator (40–42).

Accumulating evidence suggests that the actin filaments under the plasma membrane play an essential although different role in the scaffolding of specific PMCA isoforms; PSD95-induced clusters of PMCA4x/b are fenced in by the underlying actin meshwork (20), whereas NHERF2 anchors PMCA2w/b to the apical actin filaments via ezrin. It is important to note that either fencing or anchoring of PMCA clusters results in limited lateral mobility of the pumps in the plasma membrane. Disruption of the actin cytoskeleton removed the NHERF2-assembled PMCA2w/b-ezrin complex from the apical actin patches without actually disrupting the PMCA clusters, and therefore, these clusters remained virtually immobile. Our previous data on PMCA4x/b (20) and now on PMCA2w/b show that interaction with specific scaffolding proteins can assemble the different PMCA isoforms into distinct structured units that are stabilized (either fenced or anchored) by the actin cytoskeleton.

NHERF2-mediated recruitment of PMCA1b to the membrane has recently been shown to be a regulated and dynamic process; in HT-29 colon epithelial cells, endogenous PMCA1b was found to rapidly (within 60 s) translocate to the plasma membrane following muscarinic receptor stimulation, and this process was dependent on NHERF2 (39). NHERF2 translocation to the membrane preceded that of the PMCA, suggesting that regulation of NHERF2 trafficking could be a mechanism for the controlled deployment of the PMCA to specific membrane domains. In lactating breast epithelial cells, PMCA2w/b is rapidly up-regulated at the transcriptional and protein level and specifically targeted to the apical membrane where it is important for calcium enrichment of the milk (9, 10). By facilitating this process and by immobilizing the pump via ezrin linkage to the actin meshwork, NHERF2 may be responsible for maintaining the exceptionally high levels of PMCA2w/b in the apical membrane of these cells.

In conclusion, our work suggests that in polarized epithelial cells the localization, membrane density, and mobility of PMCA2b are determined by a balance between localization signals at the A-splice site (w, x, or z inserts) and interactions with scaffolding proteins mediated by the PDZ-binding C-terminal tail (see the schematic in Fig. 6) as follows. (i) Targeting of the z-splice form is not firmly determined, hence co-expression with NHERF2 can change its localization. (ii) The short insert in the x-splice form provides a strong basolateral localization signal. (iii) Insertion of 31 additional residues in the w-splice form

masks or overrides this signal and directs the pump to the apical compartment. (iv) The apical concentration and membrane stability of PMCA2w/b can be enhanced by interaction with the apical PDZ protein NHERF2. These data provide novel insights into how specific PMCA isoforms are localized and maintained in distinct calcium signaling compartments of polarized cells.

REFERENCES

1. Strehler, E. E., and Zacharias, D. A. (2001) *Physiol. Rev.* **81,** 21–50
2. Chicka, M. C., and Strehler, E. E. (2003) *J. Biol. Chem.* **278,** 18464–18470
3. Grati, M., Aggarwal, N., Strehler, E. E., and Wenthold, R. J. (2006) *J. Cell Sci.* **119,** 2995–3007
4. DeMarco, S. J., and Strehler, E. E. (2001) *J. Biol. Chem.* **276,** 21594–21600
5. Schuh, K., Uldrijan, S., Gambaryan, S., Roethlein, N., and Neyses, L. (2003) *J. Biol. Chem.* **278,** 9778–9883
6. DeMarco, S. J., Chicka, M. C., and Strehler, E. E. (2002) *J. Biol. Chem.* **277,** 10506–10511
7. Dumont, R. A., Lins, U., Filoteo, A. G., Penniston, J. T., Kachar, B., and Gillespie, P. G. (2001) *J. Neurosci.* **21,** 5066–5078
8. Burette, A., Rockwood, J. M., Strehler, E. E., and Weinberg, R. J. (2003) *J. Comp. Neurol.* **467,** 464–476
9. Reinhardt, T. A., Filoteo, A. G., Penniston, J. T., and Horst, R. L. (2000) *Am. J. Physiol. Cell Physiol.* **279,** C1595–C1602
10. Reinhardt, T. A., Lippolis, J. D., Shull, G. E., and Horst, R. L. (2004) *J. Biol. Chem.* **279,** 42369–42373
11. Fanning, A. S., and Anderson, J. M. (1999) *Curr. Opin. Cell Biol.* **11,** 432–439
12. Shenolikar, S., Voltz, J. W., Cunningham, R., and Weinman, E. J. (2004) *Physiology* **19,** 362–369
13. Meder, D., Shevchenko, A., Simons, K., and Füllekrug, J. (2005) *J. Cell Biol.* **168,** 303–313
14. Fam, S. R., Paquet, M., Castleberry, A. M., Oller, H., Lee, C. J., Traynelis, S. F., Smith, Y., Yun, C. C., and Hall, R. A. (2005) *Proc. Natl. Acad. Sci. U.S.A.* **102,** 8042–8047
15. Paquet, M., Asay, M. J., Fam, S. R., Inuzuka, H., Castleberry, A. M., Oller, H., Smith, Y., Yun, C. C., Traynelis, S. F., and Hall, R. A. (2006) *J. Biol. Chem.* **281,** 29949–29961
16. Filoteo, A. G., Elwess, N. L., Enyedi, A., Caride, A., Aung, H. H., and Penniston, J. T. (1997) *J. Biol. Chem.* **272,** 23741–23747
17. Hall, R. A., Premont, R. T., Chow, C. W., Blitzer, J. T., Pitcher, J. A., Claing, A., Stoffel, R. H., Barak, L. S., Shenolikar, S., Weinman, E. J., Grinstein, S., and Lefkowitz, R. J. (1998) *Nature* **392,** 626–630
18. Hall, R. A., Ostedgaard, L. S., Premont, R. T., Blitzer, J. T., Rahman, N., Welsh, M. J., and Lefkowitz, R. J. (1998) *Proc. Natl. Acad. Sci. U.S.A.* **95,** 8496–8501
19. Phair, R. D., Gorski, S. A., and Misteli, T. (2004) *Methods Enzymol.* **375,** 393–414
20. Padányi, R., Pászty, K., Strehler, E. E., and Enyedi, A. (2009) *Biochim. Biophys. Acta* **1793,** 1023–1032
21. Reczek, D., Berryman, M., and Bretscher, A. (1997) *J. Cell Biol.* **139,** 169–179
22. Murthy, A., Gonzalez-Agosti, C., Cordero, E., Pinney, D., Candia, C., Solomon, F., Gusella, J., and Ramesh, V. (1998) *J. Biol. Chem.* **273,** 1273–1276
23. 23 Cha, B., and Donowitz, M. (2008) *Clin. Exp. Pharmacol. Physiol.* **35,** 863–871
24. Hill, J. K., Williams, D. E., LeMasurier, M., Dumont, R. A., Strehler, E. E., and Gillespie, P. G. (2006) *J. Neurosci.* **26,** 6172–6180
25. Xiong, Y., Antalffy, G., Enyedi, A., and Strehler, E. E. (2009) *Biochem. Biophys. Res. Commun.* **384,** 32–36
26. Kip, S. N., and Strehler, E. E. (2003) *Am. J. Physiol. Renal Physiol.* **284,** F122–F132
27. Pászty, K., Antalffy, G., Penheiter, A. R., Homolya, L., Padányi, R., Iliás, A., Filoteo, A. G., Penniston, J. T., and Enyedi, A. (2005) *Biochem. J.* **391,** 687–692
28. Baggaley, E., McLarnon, S., Demeter, I., Varga, G., and Bruce, J. I. (2007) *J. Biol. Chem.* **282,** 37678–37693
29. Yun, C. H., Lamprecht, G., Forster, D. V., and Sidor, A. (1998) *J. Biol. Chem.* **273,** 25856–25863
30. Moyer, B. D., Denton, J., Karlson, K. H., Reynolds, D., Wang, S., Mickle, J. E., Milewski, M., Cutting, G. R., Guggino, W. B., Li, M., and Stanton, B. A. (1999) *J. Clin. Invest.* **104,** 1353–1361
31. Moyer, B. D., Duhaime, M., Shaw, C., Denton, J., Reynolds, D., Karlson, K. H., Pfeiffer, J., Wang, S., Mickle, J. E., Milewski, M., Cutting, G. R., Guggino, W. B., Li, M., and Stanton, B. A. (2000) *J. Biol. Chem.* **275,** 27069–27074
32. Guerra, L., Fanelli, T., Favia, M., Riccardi, S. M., Busco, G., Cardone, R. A., Carrabino, S., Weinman, E. J., Reshkin, S. J., Conese, M., and Casavola, V. (2005) *J. Biol. Chem.* **280,** 40925–40933
33. Hernando, N., Déliot, N., Gisler, S. M., Lederer, E., Weinman, E. J., Biber, J., and Murer, H. (2002) *Proc. Natl. Acad. Sci. U.S.A.* **99,** 11957–11962
34. Cunningham, R. E. X., Steplock, D., Shenolikar, S., and Weinman, E. J. (2005) *Am. J. Physiol. Renal Physiol.* **289,** F933–F938
35. Cao, T. T., Deacon, H. W., Reczek, D., Bretscher, A., and von Zastrow, M. (1999) *Nature* **401,** 286–290
36. Mahon, M. J., and Segre, G. V. (2004) *J. Biol. Chem.* **279,** 23550–23558
37. Wang, B., Bisello, A., Yang, Y., Romero, G. G., and Friedman, P. A. (2007) *J. Biol. Chem.* **282,** 36214–36222
38. Wheeler, D., Sneddon, W. B., Wang, B., Friedman, P. A., and Romero, G. (2007) *J. Biol. Chem.* **282,** 25076–25087
39. Kruger, W. A., Yun, C. C., Monteith, G. R., and Poronnik, P. (2009) *J. Biol. Chem.* **284,** 1820–1830
40. Cha, B., Kenworthy, A., Murtazina, R., and Donowitz, M. (2004) *J. Cell Sci.* **117,** 3353–3365
41. Haggie, P. M., Stanton, B. A., and Verkman, A. S. (2004) *J. Biol. Chem.* **279,** 5494–5500
42. Haggie, P. M., Kim, J. K., Lukacs, G. L., and Verkman, A. S. (2006) *Mol. Biol. Cell* **17,** 4937–4945